

NASA TECHNICAL NOTE



NASA TN D-3089

1.1

NASA TN D-3089

LOAN COPY: RETURN
AFWL (WIL-8)
Kirtland AFB, N.M.

0079903

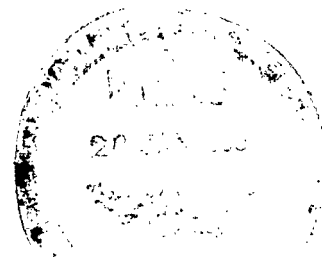


TECH LIBRARY KAFB, NM

THE GENERAL INSTABILITY OF RING-STIFFENED CORRUGATED CYLINDERS UNDER AXIAL COMPRESSION

by John N. Dickson and Richard H. Broliar

*George C. Marshall Space Flight Center
Huntsville, Ala.*



NATIONAL AERONAUTICS AND SPACE ADMINISTRATION • WASHINGTON, D. C. • JANUARY 1966



THE GENERAL INSTABILITY OF RING-STIFFENED
CORRUGATED CYLINDERS UNDER AXIAL COMPRESSION

By John N. Dickson and Richard H. Broliar

George C. Marshall Space Flight Center
Huntsville, Ala.

NATIONAL AERONAUTICS AND SPACE ADMINISTRATION

For sale by the Clearinghouse for Federal Scientific and Technical Information
Springfield, Virginia 22151 - Price \$2.00

TABLE OF CONTENTS

	Page
SUMMARY	1
INTRODUCTION.	1
GENERAL THEORY	2
Assumptions	2
Displacements and Boundary Conditions	3
Elastic Relations	3
Equilibrium Equations.	6
Determination of Buckling Load	9
COMPARISON WITH TEST RESULTS.	10
Axial Load	10
Axial Load and Bending	12
Additional Remarks	14
DISCUSSION	14
CONCLUDING REMARKS.	15
APPENDIX	23
REFERENCES	30

LIST OF ILLUSTRATIONS

Figure	Title	Page
1.	Forces and Moments Acting on Skin Element.	16
2.	Forces and Moments Acting on Ring Element	17
3.	Buckling Load Versus Mode Shape, Test Cylinder No. 1.	18
4.	General Instability Failure, Cylinder No. 4	19
5.	Ring of Cylinder No. 4	19
6.	Circumferential Mode Shape of Cylinder Tested in Axial Compression	20
7.	Ring Radial Deflection Versus Percent Load.	20
8.	Typical Strain Gage Locations	21
9.	Strain Versus Load for Test Cylinder	21
10.	Buckling Load Versus Mode Shape, Real and Apparent Minimums.	22

LIST OF TABLES

Table	Title	Page
I.	Ring-Stiffened Corrugated Cylinders - Axial Loading	11
II.	Ring-Stiffened Corrugated Cylinders - Axial and Bending Loading . .	13

DEFINITION OF SYMBOLS

Symbol	Definition
a_{ij}	matrix coefficients
c	distance from ring neutral axis to corrugation centerline, positive when rings are on outside
m	number of longitudinal half waves
n	number of circumferential waves
\overline{m}	$= m \pi / L$
\overline{n}	$= n / R$
q	buckling load per unit length of circumference, measured at corrugation centerline
t	corrugation thickness
t_x, t_y, t_s	equivalent shell thicknesses in the x and y directions and for shear, respectively per unit length of circumference
u, v, w	displacements of cylinder at corrugation centerline in x, y, and z directions, respectively
x, y, z	coordinates in axial, tangential and radial directions, respectively
A_r	area of ring
D_x	$= EI_x$
D_y, D_{xy}	circumferential bending stiffness and torsional stiffness of the corrugated cylinder, respectively
D_{yr}	$= E_r I_{yr} / L_r$
D_{zr}	$= E_r I_{zr} / L_r$
E, E_r	moduli of elasticity of corrugation and ring, respectively
\overline{E}	$= E t_x$
\overline{E}_r	$= E_r A_r / L_r$

DEFINITION OF SYMBOLS (Cont'd)

Symbol	Definition
G, G_r	shear moduli of corrugation and ring, respectively
\bar{G}	$= Gt_s$
I_x	moment of inertia of corrugation per unit length of circumference
I_{yr}	moment of inertia of ring about its centroid in plane of curvature
I_{zr}	moment of inertia of ring normal to plane of curvature
J_r	$1/G_r$ times torsional stiffness of ring
K_r	$= G_r J_r / L_r$
L	length of cylinder
L_r	ring spacing
M_x, M_y	stress couples acting on skin element in x and y directions, respectively
M_{xy}	torsional stress couple acting on skin element
M_{yr}, M_{zr}	stress couples acting on ring element in y and z directions, respectively
M_{yxr}	torsional stress couple acting on ring element
N_x, N_y	stress resultants acting on skin element in x and y directions, respectively
N_{xy}, N_{yx}	shear stress resultants acting on skin element
N_{yr}	stress resultant acting on ring element in y direction
N_{yxr}	shear stress resultant acting on ring element in x direction
Q_x, Q_y	radial shear stress resultants acting on skin element
Q_{yr}	radial shear stress resultant acting on ring element

DEFINITION OF SYMBOLS (Concluded)

Symbol	Definition
R	radius to centerline of corrugated skin
R_r	$= R + c$
T_x, T_y	moments acting at interface of skin and ring, per unit area
U, V, W	amplitudes of u, v , and w , respectively
X, Y, Z	forces acting at interface of skin and ring, per unit area
α	number of rings per longitudinal half wave length
β	bending factor, ratio of maximum buckling stress in pure bending to buckling stress in axial compression for a given cylinder
γ	ratio of maximum bending stress to maximum total stress for a cylinder under combined loading
γ_{xy}	shear strain of corrugation
ϵ_x, ϵ_y	strains of corrugation in x and y directions, respectively
ϵ_{yr}	circumferential strain of ring
θ	$= y/R$
κ_x, κ_y	curvature changes of corrugation in x and y directions, respectively
κ_{xy}	specific twist of skin element
κ_{yr}, κ_{zr}	curvature changes in plane and normal to plane of ring, respectively
κ_{yxr}	specific twist of ring
λ	$= q \bar{m}^2$
μ_x, μ_y	Poisson's ratios associated with bending in the x and y directions, respectively
μ'_x, μ'_y	Poisson's ratios associated with extension in the x and y directions, respectively
σ	longitudinal stress in corrugation

THE GENERAL INSTABILITY OF RING-STIFFENED CORRUGATED CYLINDERS UNDER AXIAL COMPRESSION

SUMMARY

A method is presented to determine the general instability load of a ring-stiffened corrugated cylinder under axial compression. This method is developed using linear small deflection theory. The stiffness properties of the rings are uniformly distributed along the cylinder and the eccentricity of the rings with respect to the corrugation centerline is taken into account.

Analytical and experimental results are compared. In this comparison good agreement is obtained for cylinders loaded in pure compression. For the cylinders subjected to bending or a combination of bending and compression the analytical calculations are conservative.

A computer program for the application of this method has been developed. The program and an explanation of its notation are included in this report.

INTRODUCTION

Axially loaded ring-stiffened corrugated cylinders are susceptible to two types of instability; panel instability and general instability. Panel instability is defined as buckling of the cylinder between rings. In general instability, the rings as well as the cylinder undergo buckling displacements. Panel instability is discussed in many textbooks and manuals; however, the same is not true for general instability.

In comparing the stiffness characteristics of a corrugated cylinder to those of a monocoque cylinder of the same weight it must be noted that the corrugated shell has a much greater longitudinal bending stiffness. This advantage is offset to some degree by the low circumferential extensional stiffness of the corrugated cylinder. Because of this lack of circumferential extensional stiffness each corrugation will act as an individual column unless the shell is reinforced by rings. Low extensional stiffness may be desirable, however, in areas of high thermal gradients.

In the past, ring-stiffened cylinders have often been designed to prevent general instability by employing semi-empirical methods to size the rings. One of the most commonly used of such methods is given by Shanley [1]. Until recently it was believed that the ring moment of inertia obtained from his formula

was sufficient to safeguard against general instability. Tests performed under the direction of the Marshall Space Flight Center as part of the Saturn V development program have shown, however, that Shanley's criterion may be very unservative for the design of ring-stiffened corrugated cylinders. The results of these tests are given in Tables I and II.

Since Shanley's work was published, considerable research has been performed on the stability of stiffened cylinders. A major contribution was made by Van der Neut [2], when he considered the effect of ring and stringer eccentricities. Additional contributions were made by Hedgepeth and Hall [3], Card [4], and Baruch and Singer [5]. Often, however, research in this field has produced a method which is either too academic or too complex to be used by the stress analyst.

The purpose of this report is to present a reliable and relatively simple means of predicting the general instability load of corrugated cylinders under axial compression. This method considers the eccentricity of the rings with respect to the corrugation centerline. It also incorporates all the stiffnesses attributable to the rings and the shear and longitudinal stiffness properties of the corrugation. The circumferential extensional and bending stiffnesses and the torsional stiffness of the corrugation are small (generally less than 1 percent of the longitudinal stiffnesses) and are therefore neglected.

GENERAL THEORY

Assumptions

The method of analysis presented in this paper is based on the following assumptions:

1. Linear small deflection theory applies. This is justified because the high longitudinal bending stiffness of a corrugated cylinder makes it less susceptible to initial imperfections and other monocoque effects.
2. The longitudinal wavelength of the buckled skin is sufficiently large to permit a "smeared" ring approach; i. e. , all the ring stiffness parameters may be uniformly distributed along the cylinder.
3. The corrugated cylinder can be treated as an equivalent orthotropic cylinder, the radius of which is equal to the mean radius of the corrugation.

4. The circumferential extensional and bending stiffnesses of the corrugation as well as its torsional stiffness can be neglected since they are small as compared to the longitudinal stiffness properties of the shell.

5. Buckling displacements are sinusoidal.

6. Prebuckling deformations are neglected.

7. Plasticity effects and local failures are not considered.

Displacements and Boundary Conditions

The cylinder is in equilibrium under the applied load just prior to buckling and deformations due to buckling are measured from this position. In accordance with assumption 5, displacements may be written in the form

$$\begin{aligned} u &= U \cos \frac{m\pi x}{L} \cos n\theta \\ v &= V \sin \frac{m\pi x}{L} \sin n\theta \\ w &= W \sin \frac{m\pi x}{L} \cos n\theta \end{aligned} \tag{1}$$

This corresponds to the following simply supported boundary conditions at $x = 0, L$

$$\begin{aligned} w &= 0 & N_x &= 0 \\ v &= 0 & M_x &= 0 \end{aligned}$$

Thus, at the ends of the cylinder motion radially and tangentially is prevented, while longitudinal motion is allowed; i.e., $u \neq 0$. These boundary conditions are appropriate for cylinders bounded by deep supporting rings, which are rigid in their own planes but may readily bend or warp out of their planes.

Elastic Relations

For an orthotropic shell the relations for the stress resultants and couples in terms of the strains and curvatures are

$$\begin{aligned}
N_x &= \frac{Et_x}{1 - \mu'_x \mu'_y} (\epsilon_x + \mu'_y \epsilon_y) \\
N_y &= \frac{Et_y}{1 - \mu'_x \mu'_y} (\epsilon_y + \mu'_x \epsilon_x) \\
N_{xy} &= \bar{G} \gamma_{xy} \\
M_x &= \frac{D_x}{1 - \mu_x \mu_y} (\kappa_x + \mu_y \kappa_y) \\
M_y &= \frac{D_y}{1 - \mu_x \mu_y} (\kappa_y + \mu_x \kappa_x) \\
M_{xy} &= D_{xy} \kappa_{xy}
\end{aligned} \tag{2}$$

In view of assumption (4) and with the use of the reciprocal theorem, equations (2) lead directly to the following expressions for the corrugated cylinder

$$\begin{aligned}
N_x &= \bar{E} \epsilon_x = \bar{E} \frac{\partial u}{\partial x} \\
N_{xy} &= \bar{G} \left(\frac{1}{R} \frac{\partial u}{\partial \theta} + \frac{\partial v}{\partial x} \right) \\
M_x &= D_x \kappa_x = D_x \frac{\partial^2 w}{\partial x^2} \\
N_y &= M_y = M_{xy} = 0
\end{aligned} \tag{3}$$

The rings are considered eccentric with respect to the centerline of the skin and displacements of the ring at its centroid may be found by means of the transformations

$$\begin{aligned}
u_r &= u - c \frac{\partial w}{\partial x} \\
v_r &= \frac{R}{R} v - \frac{c}{R} \frac{\partial w}{\partial \theta} \\
w_r &= w
\end{aligned} \tag{4}$$

where c is the distance from the ring centroid to the skin centerline. For a ring loaded normal to, as well as in the plane of, initial curvature, the strain, curvatures and specific twist at the central axis, may be written

$$\begin{aligned}
 \epsilon_{yr} &= \frac{1}{R_r} \left(\frac{\partial v_r}{\partial \theta} + w_r \right) \\
 \kappa_{yr} &= \frac{1}{R_r^2} \left(\frac{\partial^2 w_r}{\partial \theta^2} - \frac{\partial v_r}{\partial \theta} \right) \\
 \kappa_{zr} &= \frac{1}{R_r^2} \left(\frac{\partial^2 u_r}{\partial \theta^2} - R_r \frac{\partial w_r}{\partial x} \right) \\
 \kappa_{yxr} &= \frac{1}{R_r^2} \left(R_r \frac{\partial^2 w_r}{\partial x \partial \theta} + \frac{\partial u_r}{\partial \theta} \right)
 \end{aligned} \tag{5}$$

Assuming the shear center to coincide with the ring centroid, the stress resultants and stress couples acting on an element of the ring are related to the strains and curvatures by the equations

$$\begin{aligned}
 N_{yr} &= \bar{E}_r \epsilon_{yr} \\
 M_{yr} &= D_{yr} \kappa_{yr} \\
 M_{zr} &= D_{zr} \kappa_{zr} \\
 M_{yxr} &= K_r \kappa_{yxr}
 \end{aligned}$$

Substituting equations (4) and (5) in the above expressions gives

$$\begin{aligned}
 N_{yr} &= \bar{E}_r \left[\frac{1}{R} \frac{\partial v}{\partial \theta} + \frac{1}{R_r} \left(w - \frac{c}{R} \frac{\partial^2 w}{\partial \theta^2} \right) \right] \\
 M_{yr} &= \frac{D_{yr}}{R R_r} \left(- \frac{\partial v}{\partial \theta} + \frac{\partial^2 w}{\partial \theta^2} \right) \\
 M_{zr} &= \frac{D_{zr}}{R_r^2} \left[\frac{\partial^2 u}{\partial \theta^2} - \frac{\partial}{\partial x} \left(R_r w + c \frac{\partial^2 w}{\partial \theta^2} \right) \right]
 \end{aligned} \tag{6}$$

$$M_{yxr} = \frac{K_r}{R^2_r} \left(\frac{\partial u}{\partial \theta} + R \frac{\partial^2 w}{\partial x \partial \theta} \right) \quad (6 \text{ concluded})$$

Equilibrium Equations

Differential equations are obtained by considering separately the equilibrium of an element of the skin and a corresponding "smeared" ring element. Six conditions of equilibrium must be satisfied by the forces and moments acting on each of the elements. An element of the skin is shown in Figure 1 a, b, c. The first of these figures shows the stress resultants and the forces X, Y, and Z acting at the interface of the skin and the ring, and the second figure gives the stress couples and the moments T_x and T_y transferred into the skin element from the ring. Components of the buckling force resulting from the deformation of the element are shown in Figure 1c. The component in the x direction is multiplied by the quantity $(1 + \epsilon_x)$ to include the straining of the middle surface as suggested by Flügge (7). The components in the y and z directions are due to the rotations $\partial v / \partial x$ and $\partial w / \partial x$ of the element respectively.

The six conditions of equilibrium for the skin lead to the following equations

$$\begin{aligned} \frac{\partial N_x}{\partial x} + \frac{1}{R} \frac{\partial N_{yx}}{\partial \theta} - q \frac{\partial^2 u}{\partial x^2} + X &= 0 \\ \frac{\partial N_{xy}}{\partial x} - q \frac{\partial^2 v}{\partial x^2} + Y &= 0 \\ \frac{\partial Q_x}{\partial x} - q \frac{\partial^2 w}{\partial x^2} + Z &= 0 \\ \frac{\partial M_x}{\partial x} + Q_x + T_x &= 0 \\ T_y &= 0 \\ N_{xy} - N_{yx} &= 0 \end{aligned} \quad (7)$$

These equations may be combined and put in the form

$$\begin{aligned}
X &= -\frac{\partial N_x}{\partial x} - \frac{1}{R} \frac{\partial N_{yx}}{\partial \theta} + q \frac{\partial^2 u}{\partial x^2} \\
Y - \frac{T_y}{R} &= -\frac{\partial N_{yx}}{\partial x} + q \frac{\partial^2 v}{\partial x^2} \\
Z - \frac{\partial T_x}{\partial x} - \frac{1}{R} \frac{\partial T_y}{\partial \theta} &= \frac{\partial^2 M_x}{\partial x^2} + q \frac{\partial^2 w}{\partial x^2}
\end{aligned} \tag{8}$$

The six equations of equilibrium for an element of the ring (Fig. 2) may be obtained in a similar manner. They are

$$\begin{aligned}
\frac{1}{R} \frac{\partial N_{yxr}}{\partial \theta} &= -X = 0 \\
\frac{1}{R} \frac{\partial N_{yr}}{\partial \theta} + \frac{Q_{yr}}{R} &= -Y = 0 \\
\frac{1}{R} \frac{\partial Q_{yr}}{\partial \theta} - \frac{N_{yr}}{R} &= -Z = 0 \\
\frac{1}{R} \frac{\partial M_{yxr}}{\partial \theta} - \frac{c}{R} \frac{\partial N_{yxr}}{\partial \theta} + \frac{M_{zr}}{R} - T_x &= 0 \\
\frac{1}{R} \frac{\partial M_{yr}}{\partial \theta} - \frac{c}{R} \frac{\partial N_{yr}}{\partial \theta} + Q_{yr} - T_y &= 0 \\
R_r N_{yxr} + \frac{\partial M_{zr}}{\partial \theta} - M_{yxr} &= 0
\end{aligned} \tag{9}$$

The last three of the above equations are used to eliminate Q_{yr} and N_{yxr} . This yields the following three equations

$$\begin{aligned}
X &= -\frac{1}{R R_r} \frac{\partial^2 M_{zr}}{\partial \theta^2} + \frac{1}{R R_r} \frac{\partial M_{yxr}}{\partial \theta} \\
Y - \frac{T_y}{R} &= \frac{R_r}{R^2} \frac{\partial N_{yr}}{\partial \theta} - \frac{1}{R^2} \frac{\partial M_{yr}}{\partial \theta} \\
Z - \frac{\partial T_x}{\partial x} - \frac{1}{R} \frac{\partial T_y}{\partial \theta} &= -\frac{N_{yr}}{R} + \frac{c}{R^2} \frac{\partial^2 N_{yr}}{\partial \theta^2} \\
&\quad - \frac{1}{R_r} \frac{\partial^2 M_{yxr}}{\partial x \partial \theta} - \frac{1}{R} \frac{\partial}{\partial x} \left(M_{zr} + \frac{c}{R_r} \frac{\partial^2 M_{zr}}{\partial \theta^2} \right) - \frac{1}{R^2} \frac{\partial^2 M_{yr}}{\partial \theta^2}
\end{aligned} \tag{10}$$

The forces X , Y , and Z and the moments T_x and T_y acting at the interface of the skin and ring may now be eliminated by subtracting equation (8) from equation (10). Hence,

$$\begin{aligned}
& \frac{\partial N_x}{\partial x} + \frac{1}{R} \frac{\partial N_{yx}}{\partial \theta} - \frac{1}{R R_r} \frac{\partial^2 M_{zr}}{\partial \theta^2} + \frac{1}{R R_r} \frac{\partial M_{yxr}}{\partial \theta} - q \frac{\partial^2 u}{\partial x^2} = 0 \\
& \frac{\partial N_{yx}}{\partial x} + \frac{R_r}{R^2} \frac{\partial N_{yr}}{\partial \theta} - \frac{1}{R^2} \frac{\partial M_{yr}}{\partial \theta} - q \frac{\partial^2 v}{\partial x^2} = 0 \\
& - \frac{\partial^2 M_x}{\partial x^2} - \frac{N_{yr}}{R} + \frac{c}{R^2} \frac{\partial^2 N_{yr}}{\partial \theta^2} - \frac{1}{R^2} \frac{\partial^2 M_{yr}}{\partial \theta^2} - \frac{1}{R_r} \frac{\partial^2 M_{yxr}}{\partial x \partial \theta} \\
& - \frac{1}{R} \frac{\partial M_{zr}}{\partial x} - \frac{c}{R R_r} \frac{\partial^3 M_{zr}}{\partial x \partial \theta^2} - q \frac{\partial^2 w}{\partial x^2} = 0
\end{aligned} \tag{11}$$

These are the equilibrium equations in terms of the stress resultants. Substituting the expressions (3) and (6) for the stress resultants into equations (11) gives the equilibrium equations in terms of the displacements.

$$\begin{aligned}
& \bar{E} \frac{\partial^2 u}{\partial x^2} + \frac{\bar{G}}{R^2} \left(\frac{\partial^2 u}{\partial \theta^2} + R \frac{\partial^2 v}{\partial x \partial \theta} \right) + \frac{D_{zr}}{R R_r^3} \left(- \frac{\partial^4 u}{\partial \theta^4} + R_r \frac{\partial^3 w}{\partial x \partial \theta^2} + c \frac{\partial^5 w}{\partial x \partial \theta^4} \right) \\
& + \frac{K_r}{R R_r^3} \left(\frac{\partial^2 u}{\partial \theta^2} + R \frac{\partial^3 w}{\partial x \partial \theta^2} \right) - q \frac{\partial^2 u}{\partial x^2} = 0 \\
& \bar{G} \left(\frac{1}{R} \frac{\partial^2 u}{\partial x \partial \theta} + \frac{\partial^2 v}{\partial x^2} \right) + \bar{E}_r \left(\frac{R_r}{R^3} \frac{\partial^2 v}{\partial \theta^2} + \frac{1}{R^2} \frac{\partial w}{\partial \theta} - \frac{c}{R^3} \frac{\partial^3 w}{\partial \theta^3} \right) \\
& + \frac{D_{yr}}{R^3 R_r} \left(\frac{\partial^2 v}{\partial \theta^2} - \frac{\partial^3 w}{\partial \theta^3} \right) - q \frac{\partial^2 v}{\partial x^2} = 0 \\
& -D_x \frac{\partial^4 w}{\partial x^4} + \frac{\bar{E}_r}{R^2} \left(- \frac{\partial v}{\partial \theta} + \frac{c}{R} \frac{\partial^3 v}{\partial \theta^3} - \frac{R_r}{R} w + \frac{2c}{R_r} \frac{\partial^2 w}{\partial \theta^2} - \frac{c^2}{R R_r} \frac{\partial^4 w}{\partial \theta^4} \right) \\
& + \frac{D_{yr}}{R^3 R_r} \left(\frac{\partial^3 v}{\partial \theta^3} - \frac{\partial^4 w}{\partial \theta^4} \right) - \frac{K_r}{R^3} \left(\frac{\partial^3 u}{\partial x \partial \theta^2} + R \frac{\partial^4 w}{\partial x^2 \partial \theta^2} \right) - \frac{D_{zr}}{R R_r^2} \left(\frac{\partial^3 u}{\partial x \partial \theta^2} + \right. \\
& \left. \frac{c}{R_r} \frac{\partial^5 u}{\partial x \partial \theta^4} - R_r \frac{\partial^2 w}{\partial x^2} - 2c \frac{\partial^4 w}{\partial x^2 \partial \theta^2} - \frac{c^2}{R_r} \frac{\partial^6 w}{\partial x^2 \partial \theta^4} \right) - q \frac{\partial^2 w}{\partial x^2} = 0
\end{aligned} \tag{12}$$

After introducing the expression for the displacements given by equations (1) into the differential equations (12) one obtains the following three linear equations.

$$\begin{aligned}
& - \left[\bar{E} \bar{m}^2 + \bar{G} \bar{n}^2 + D_{zr} \left(\frac{R}{R_r} \right)^3 \bar{n}^4 + \frac{K_r R}{R_r^3} \bar{n}^2 \right] U + \left[\bar{G} \bar{m} \bar{n} \right] V \\
& - \left[D_{zr} \left(\frac{R}{R_r} \right)^3 \left(\frac{R_r}{R^2} - c \bar{n}^2 \right) \bar{m} \bar{n}^2 + \frac{K_r}{R} \left(\frac{R}{R_r} \right)^3 \bar{m} \bar{n}^2 \right] W + q \bar{m}^2 U = 0 \\
& \left[\bar{G} \bar{m} \bar{n} \right] U - \left[\bar{G} \bar{m}^2 + \bar{E}_r \frac{R_r}{R} \bar{n}^2 + \frac{D_{yr}}{R_r R} \bar{n}^2 \right] V \\
& - \left[\bar{E}_r \bar{n} \left(\frac{1}{R} + c \bar{n}^2 \right) + \frac{D_{yr}}{R_r} \bar{n}^3 \right] W + q \bar{m}^2 V = 0 \tag{13} \\
& - \left[D_{zr} \left(\frac{R}{R_r} \right)^3 \left(\frac{R_r}{R^2} - c \bar{n}^2 \right) \bar{m} \bar{n}^2 + \frac{K_r}{R} \left(\frac{R}{R_r} \right)^3 \bar{m} \bar{n}^2 \right] U \\
& - \left[\bar{E}_r \bar{n} \left(\frac{1}{R} + c \bar{n}^2 \right) + \frac{D_{yr}}{R_r} \bar{n}^3 \right] V - \left[\bar{E}_r \left(\frac{R}{R_r} \right) \left(\frac{1}{R} + c \bar{n}^2 \right)^2 + D_x \bar{m}^4 \right. \\
& \left. + D_{yr} \left(\frac{R}{R_r} \right) \bar{n}^4 + D_{zr} \left(\frac{R}{R_r} \right)^3 \left(\frac{R_r}{R^2} - c \bar{n}^2 \right)^2 \bar{m}^2 + K_r \left(\frac{R}{R_r} \right)^3 \bar{m}^2 \bar{n}^2 \right] W \\
& + q \bar{m}^2 W = 0
\end{aligned}$$

Determination of Buckling Load

The set of homogeneous equations (13) has nontrivial solutions only when the determinant of its matrix is zero. Equations (13) may be written in matrix form

$$\begin{bmatrix} a_{11} + \lambda & a_{12} & a_{13} \\ a_{21} & a_{22} + \lambda & a_{23} \\ a_{31} & a_{32} & a_{33} + \lambda \end{bmatrix} \begin{bmatrix} U \\ V \\ W \end{bmatrix} = 0 \tag{14}$$

The determinant of the characteristic matrix of A is a polynomial of the third degree in λ . The problem of determining the buckling load ($q = \lambda/\overline{m}^2$) for known values of m and n has therefore been reduced to that of finding the roots (eigenvalues) of the characteristic equation

$$a + b\lambda + c\lambda^2 + \lambda^3 = 0 \quad (15)$$

where a, b, and c are known functions of the coefficients a_{ij} . Obviously only real and positive roots of equation (15) are of interest, the lowest of which determines the buckling load for the mode shape under consideration. The critical buckling load of the cylinder may be found by calculating q for a range of values of m and n, and plotting a family of curves as shown in Figure 3. The critical buckling load will then be the minimum value of q corresponding to integer values of m and n. If the computer program (see Appendix) is used, the minimum buckling load will be indicated for the specified range of m and n, and no plotting is required.

Since W is usually in the order of n times larger than V or U an approximate solution for q may be obtained by dropping the terms containing q in the first two of equations (13). This yields

$$q_{m,n} = \frac{|A|}{(a_{12}^2 - a_{11} a_{22}) \overline{m}^2} \quad (16)$$

where $|A|$ is the determinant of the symmetrical matrix

$$\begin{bmatrix} a_{11} & a_{12} & a_{13} \\ a_{12} & a_{22} & a_{23} \\ a_{13} & a_{23} & a_{33} \end{bmatrix}$$

If an iterative procedure is used to find the roots of equation (15), the above approximation is found to be very useful as a starting point.

COMPARISON WITH TEST RESULTS

Axial Load

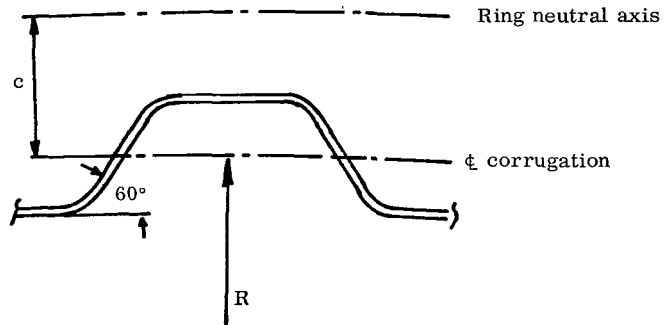
As a part of the Saturn V development program eleven ring-stiffened corrugated cylinders were tested to failure under axial load. Of these, five

failed in general instability. The remaining cylinders failed either by panel instability or local crippling before the general instability load was reached. A photograph of a typical general instability failure is shown in Figure 4. Figure 5 shows one of the rings of this cylinder after the failure. Table I gives the geometries of these five cylinders along with their actual and calculated failure loads. The close agreement between the experimental data and calculations supports the validity of the method of analysis given in this report.

TABLE I. RING-STIFFENED CORRUGATED CYLINDERS - AXIAL LOADING

CYLINDER	No. 1	No. 2	No. 3	No. 4	No. 5
Aluminum Alloy	7075-T6	7075-T6	7075-T6	7075-T6	7075-T6
Cylinder Length (in.)	33.0	33.0	33.0	69.6	69.6
(cm)	83.8	83.8	83.8	176.8	176.8
Radius (in.)	24.7	24.7	24.7	49.4	49.4
(cm)	62.7	62.7	62.7	125.0	125.0
Corrugation Pitch (in.)	1.43	1.43	1.43	2.85	2.85
(cm)	3.63	3.63	3.63	7.24	7.24
Corrugation Thickness (in.)	0.020	0.019	0.025	0.041	0.041
(cm)	0.05	0.048	0.06	0.10	0.10
Corrugation Depth (in.)	0.44	0.44	0.44	0.87	0.87
(cm)	1.12	1.12	1.12	2.21	2.21
Type of Ring	\mathbf{C}^*	\mathbf{I}	\mathbf{I}	\mathbf{I}	\mathbf{I}
Ring Spacing (in.)	6.38	6.38	6.38	12.4	12.4
(cm)	16.21	16.21	16.21	31.5	31.5
Ring Moment of Inertia (in. ⁴)	0.0050	0.0104	0.0104	0.286	0.286
(cm ⁴)	0.208	0.433	0.433	11.9	11.9
Ring Area (in. ²)	0.040	0.121	0.121	0.180	0.180
(cm ²)	0.258	0.78	0.78	1.16	1.16
Ring Eccentricity (in.)	-0.73	-0.53	-0.53	-1.99	-1.99
(cm)	-1.85	-1.35	-1.35	-5.05	-5.05
Actual Failure Load (Kips)	131.	174.	224.	659.	648.
(N)	5.83×10^5	7.74×10^5	9.96×10^5	2.93×10^6	2.88×10^6
Calculated Failure Load (Kips)	118.	198.	233.	654.	654.
(N)	5.25×10^5	8.81×10^5	1.04×10^6	2.91×10^5	2.91×10^6
Percent Error (%)	11.0	-12.1	-3.9	0.8	-0.9

* For this ring an effective moment of inertia and effective area were calculated using the approach given in Reference 9.



The instrumentation on these cylinders provided some interesting information. The radial deflection gages located on the rings showed that as the load increased most of the rings deflected into the theoretically predicted circumferential mode shape. Figure 6 shows a typical example of this phenomenon. When the radial deflection at a point of maximum bending on the ring is plotted versus axial load the curve obtained is asymptotic to the failure load as is shown in Figure 7.

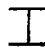
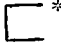
Another interesting phenomenon was shown by the strain gages located on the corrugated skin. Two gages were located opposite each other at various points on the skin, see Figure 8, so that longitudinal bending of the corrugation could be observed. As the axial load on the cylinder increased, the strain versus load plot of the two gages in each set remained linear and almost coincident until just below the failure load. Then at various locations on the cylinder the strain in one gage increased nonlinearly while the strain in the other leveled off and then decreased as shown in Figure 9. This meant that the corrugation was bending appreciably, and failure of the cylinder was imminent. The actual cylinder failures were similar to monocoque failures in their swiftness. Conjecture can be made that this second phenomenon might be used to determine the general instability failure load of a ring-stiffened corrugated cylinder without actually failing the specimen.

Axial Load and Bending

Test data is also available for a ring-stiffened corrugated cylinder loaded in pure bending and for a cylinder loaded simultaneously in bending and axial compression. Table II gives the cylinder geometries and loads. Cylinders loaded in the above manner are usually analyzed by calculating the maximum compressive stress due to bending and axial load and then assuming this stress to act along the entire periphery of the cylinder. This, however, leads to a conservative prediction for the buckling stress, since a stiffened cylinder can withstand a greater maximum stress in bending than in pure compression. This increased load carrying capability of cylinders in bending can be expressed in terms of a bending factor, β . If the bending factor β and the allowable stress in pure compression σ are known then the maximum allowable stress in any combination of bending and compression may be calculated from the equation

$$\sigma_{\max} = \frac{\sigma}{1 - \gamma \left(1 - \frac{1}{\beta}\right)}$$

**TABLE II. RING-STIFFENED CORRUGATED CYLINDERS -
AXIAL AND BENDING LOADING**

CYLINDERS	No. 6	No. 7
Aluminum Alloy	7075-T6	7075-T6
Cylinder Length (in.)	268.6	33.0
(cm)	682.2	83.8
Radius (in.)	197.6	24.7
(cm)	501.9	62.7
Corrugation Thickness (in.)	0.145	0.020
(cm)	0.368	0.051
Corrugation Pitch (in.)	11.40	1.43
(cm)	28.95	3.63
Corrugation Depth (in.)	3.48	0.44
(cm)	8.84	1.12
Type of Ring		 *
Ring Spacing (in.)	51.0	6.38
(cm)	129.54	16.20
Ring In-Plane Moment of Inertia (in. ⁴)	34.4	0.0050
(cm ⁴)	0.1431	0.208
Ring Out-of-Plane Moment of Inertia (in. ⁴)	0	0
(cm ⁴)	0	0
Ring Torsional Stiffness/G _R (in. ⁴)	0	0
(cm ⁴)	0	0
Ring Area (in. ²)	2.48	0.040
(cm ²)	16.00	0.258
Ring Eccentricity (in.)	-6.24	-0.73
(cm)	-15.84	-1.85
Actual Bending Load (Kip-ft.)	27,900	161.0
(N-m)	3.79 x 10 ⁷	2.18 x 10 ⁵
Actual Axial Load (Kips)	6,930	0
(N)	30.8 x 10 ⁶	0
Actual Maximum Stress (lb./in. ²)	43,530	37,960
(N/m ²)	3.00 x 10 ⁸	2.62 x 10 ⁸
Calculated Maximum Stress without Bending Factor (lb./in. ²)	37,560	28,620
(N/m ²)	2.59 x 10 ⁸	1.97 x 10 ⁸
Percent Error (%)	15.9	32.6
β	1.20	1.20
γ	.328	1.0
Calculated Maximum Stress with Bending Factor (lb./in. ²)	39,700	34,300
(N/m ²)	2.74 x 10 ⁸	2.36 x 10 ⁸
Percent Error (%)	9.6	10.7

* For this ring an effective moment of inertia and effective area were calculated using the approach given in reference 9.

where γ is the ratio of the bending stress to the maximum total stress. Table II shows the calculated maximum stress for these cylinders both without and with the bending factor β . For the latter, β has been taken as 1.20 which is the ratio of the actual failure stress of cylinder No. 7 to the actual failure stress of cylinder No. 1. These cylinders are identical; one was tested in bending and the other in compression.

Additional Remarks

The average number of rings (α) per longitudinal half wavelength for the cylinders given in Tables I and II is relatively low, α varying from 1.7 for cylinders No. 2 and No. 3 to 2.6 for cylinder No. 6. Van der Neut [6] performed a study to determine what error is produced by using a "smeared" ring approach when α is low. He states that for stiffened cylinders the error is on the order of 4 percent for $\alpha = 2.0$ and 6 percent for $\alpha = 1.6$, the exact error being dependent upon the cylinder stiffness properties.

All the cylinders given in Tables I and II had some end fixity. Deflection measurements indicate that for cylinders No. 4, 5, and 6 the amount of end fixity was negligible. Unfortunately there were not sufficient deflection measurements on the other cylinders to determine the amount of end fixity, but it is believed to be small for these cylinders also.

DISCUSSION

The method for predicting general instability developed in this report considers the eccentricity of the ring with respect to the skin centerline. It can be shown that this factor has a large effect on the general instability failure load. In fact, moving the rings from the inside to the outside of the cylinder can sometimes change the general instability load 100 percent or more. As an example, the general instability failure load of cylinder No. 4 is 654 kips (2.9×10^6 N) for inside rings and 1254 kips (5.6×10^6 N) if the same rings are on the outside of the corrugation. This same type of effect is present in cylinders with inside or outside longitudinal stiffeners as is shown by the test data in reference 4.

As the test results show, good agreement is obtained for the cylinders loaded in bending and for those loaded simultaneously in bending and axial compression, if a bending factor of 1.20 is applied to the bending portion of the load. Cylinders loaded in bending carry a greater maximum stress because the portion of the cylinder that is highly loaded is stabilized by the remainder of the cylinder. At the present, though, sufficient information is not available as to exactly what bending factor should be used for each particular cylinder, this factor being a function of the cylinder stiffness properties. Based on currently available information, it is not recommended that a bending factor be used for design.

The use of linear small deflection theory has been justified because the relatively high bending stiffness of a corrugated shell makes the cylinder less susceptible to initial imperfections and other monocoque effects. A corrugated shell for which this assumption does not hold true is not envisioned as being practical, but still it would be possible to make a cylinder with such a small corrugation depth that it would actually approach monocoque in properties. For a design of this nature a reduction factor will have to be applied to the failure load given by this method. An acceptable technique for determining the reduction factor is given by Almroth [8] .

For all the cylinders tested the ring extensional and in-plane bending stiffnesses were the only ring properties affecting the failure load. It is believed by the authors that for most practical applications the out-of-plane bending stiffness and the torsional stiffness of the ring are of secondary importance.

In computing the stiffness properties of the ring, care should be taken by the analyst that the effective rather than the apparent stiffness properties are used. This is especially true for the out-of-plane properties such as the lateral bending and torsional stiffness, but may also be important for the in-plane properties of the ring; e.g. a channel section having wide and comparatively thin flanges may not be fully effective in bending, as is discussed in reference 9.

It should also be mentioned that the method given in this report only determines the general instability failure load. It does not check for panel buckling or local crippling failures.

CONCLUDING REMARKS

Linear small deflection theory has been used to develop a method to determine the general instability load of a ring-stiffened corrugated cylinder under axial compression. The general instability failure loads of seven corrugated cylinders have been compared with loads calculated by using this method. Agreement between the calculated and actual failure loads were quite close for the five cylinders loaded in pure compression. When a bending factor of 1.20 was used, good agreement was also obtained for one cylinder loaded in pure bending and for one cylinder having a combination of axial and bending load. Since calculations must be made for many different mode shapes before the minimum buckling load can be determined, a computer program was developed.

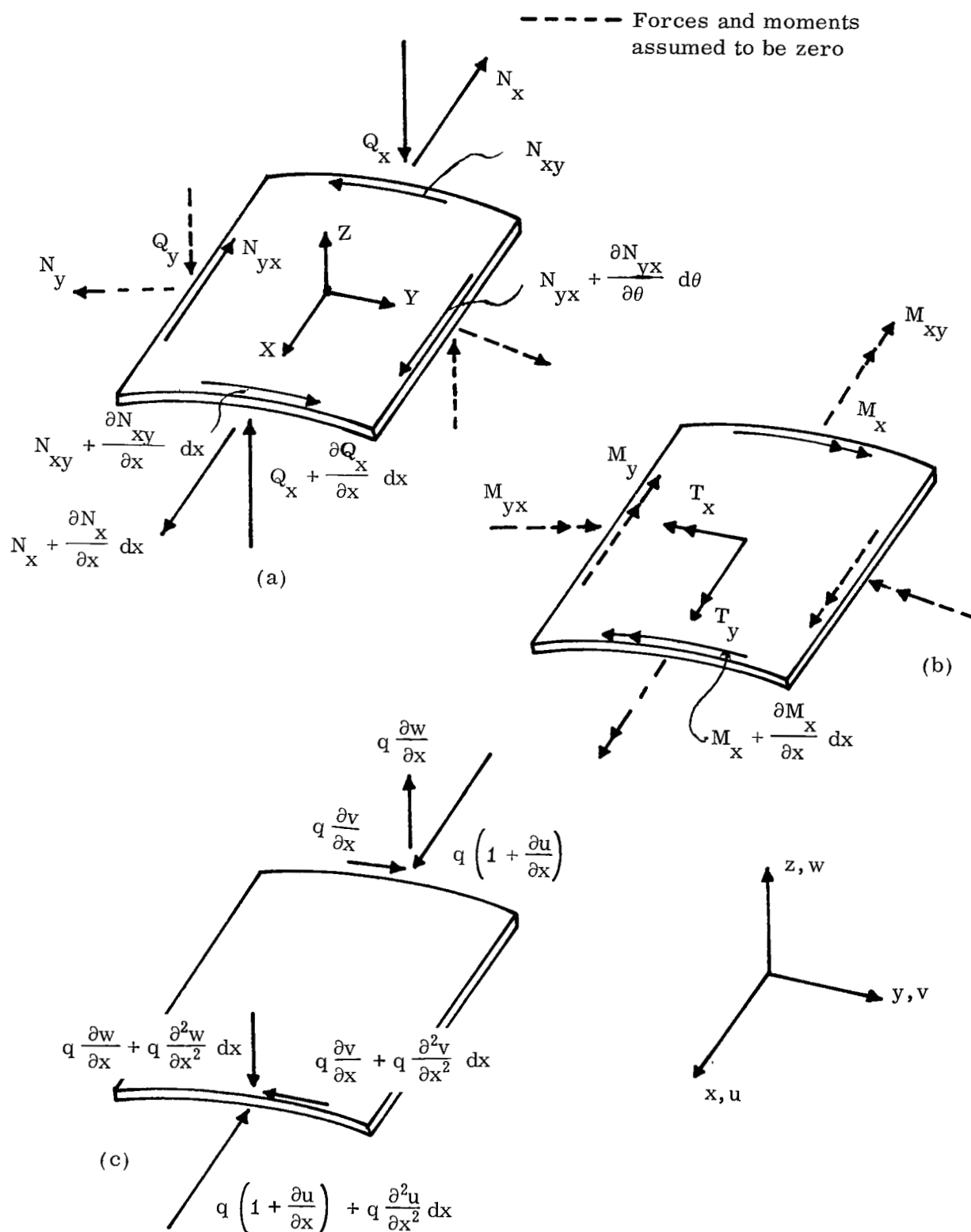


FIGURE 1. FORCES AND MOMENTS ACTING ON SKIN ELEMENT

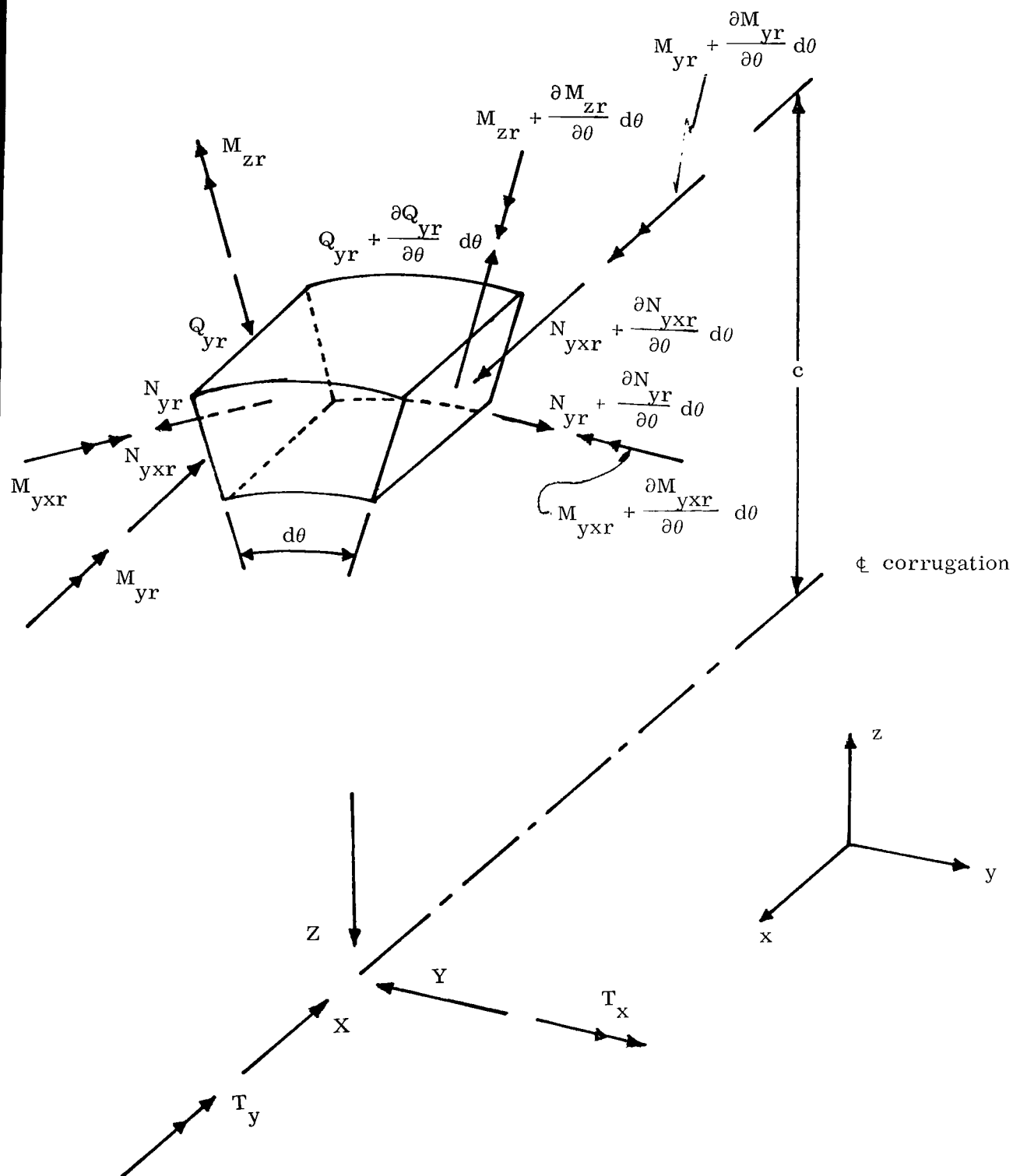


FIGURE 2. FORCES AND MOMENTS ACTING ON RING ELEMENT

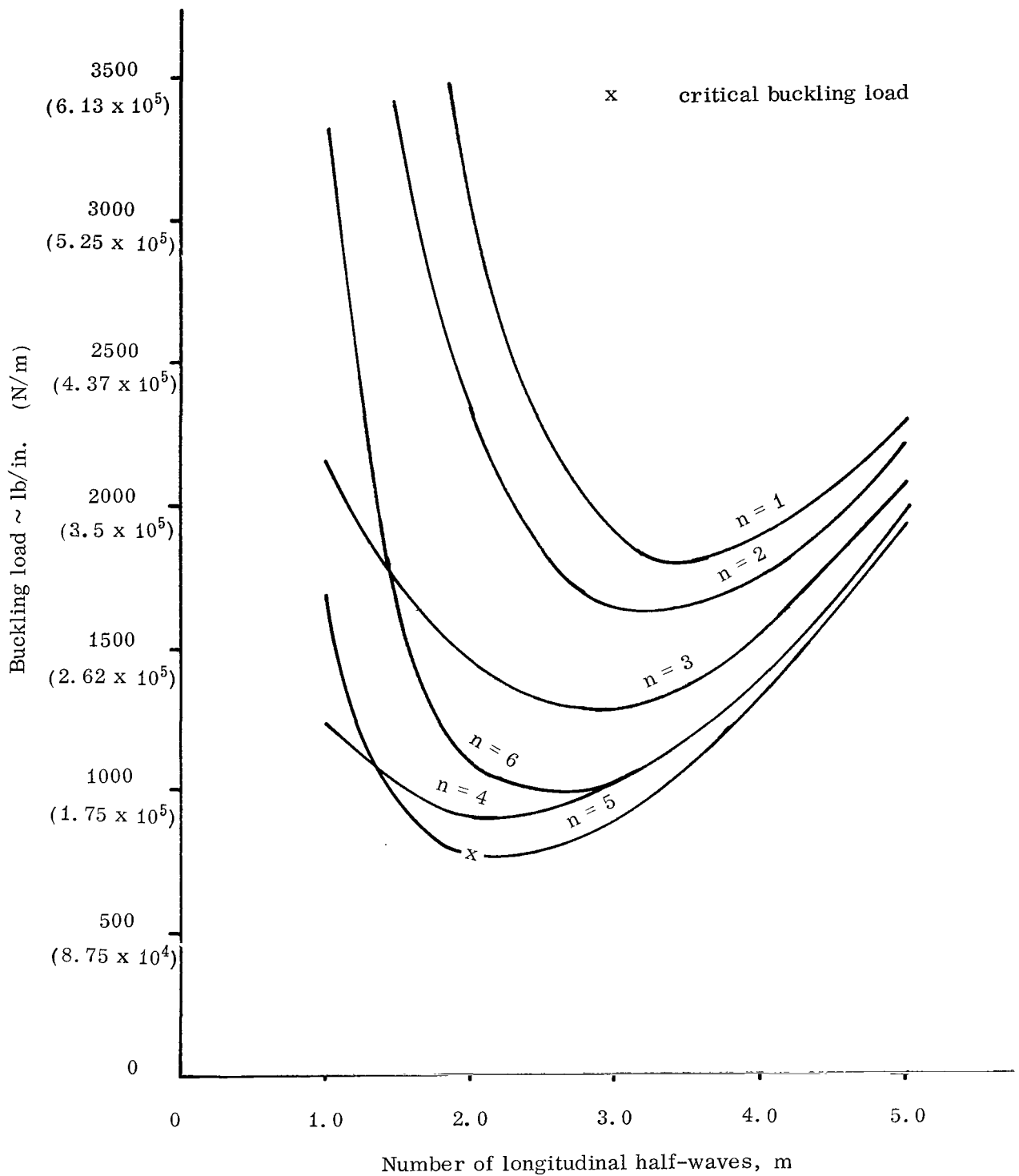


FIGURE 3. BUCKLING LOAD VERSUS MODE SHAPE, TEST CYLINDER NO. 1

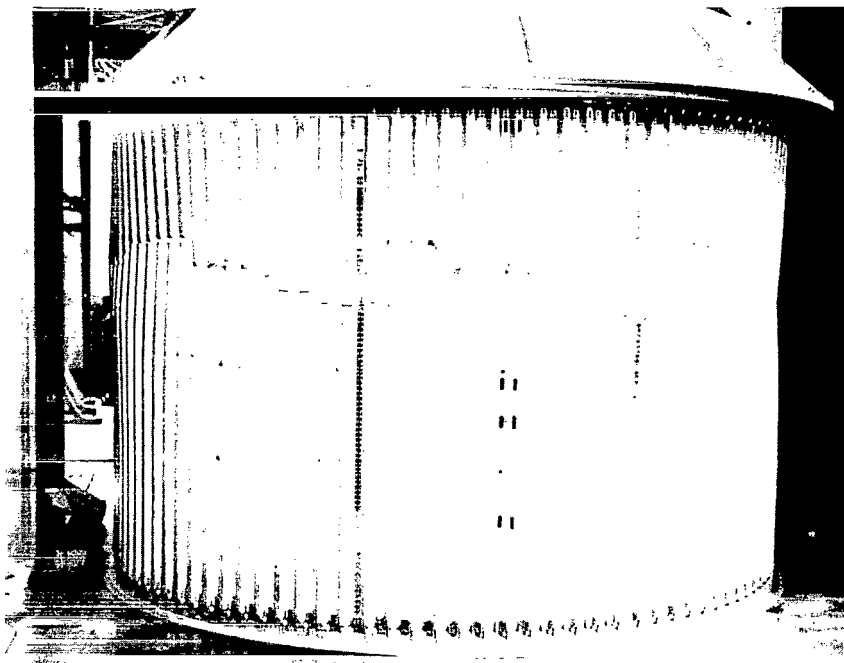


FIGURE 4. GENERAL INSTABILITY FAILURE, CYLINDER NO. 4

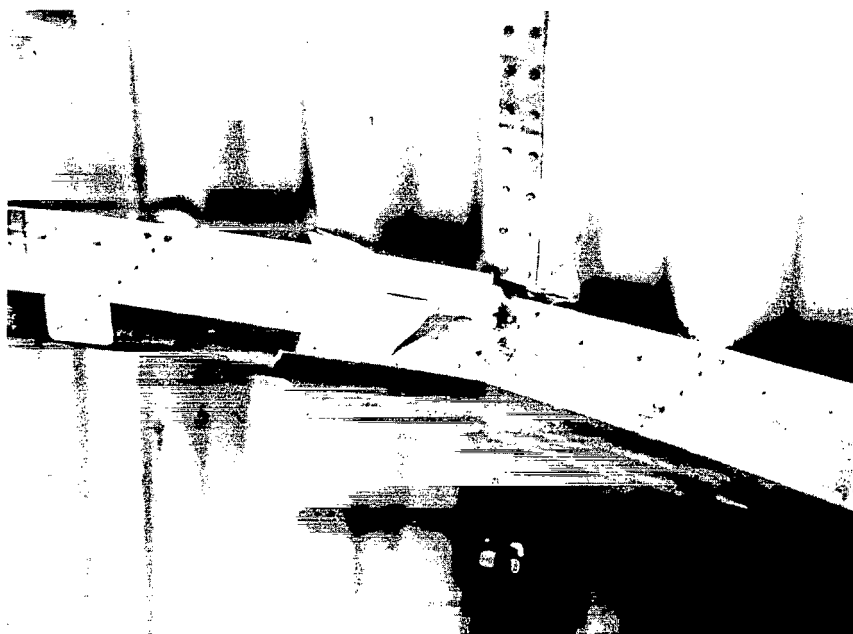


FIGURE 5. RING OF CYLINDER NO. 4

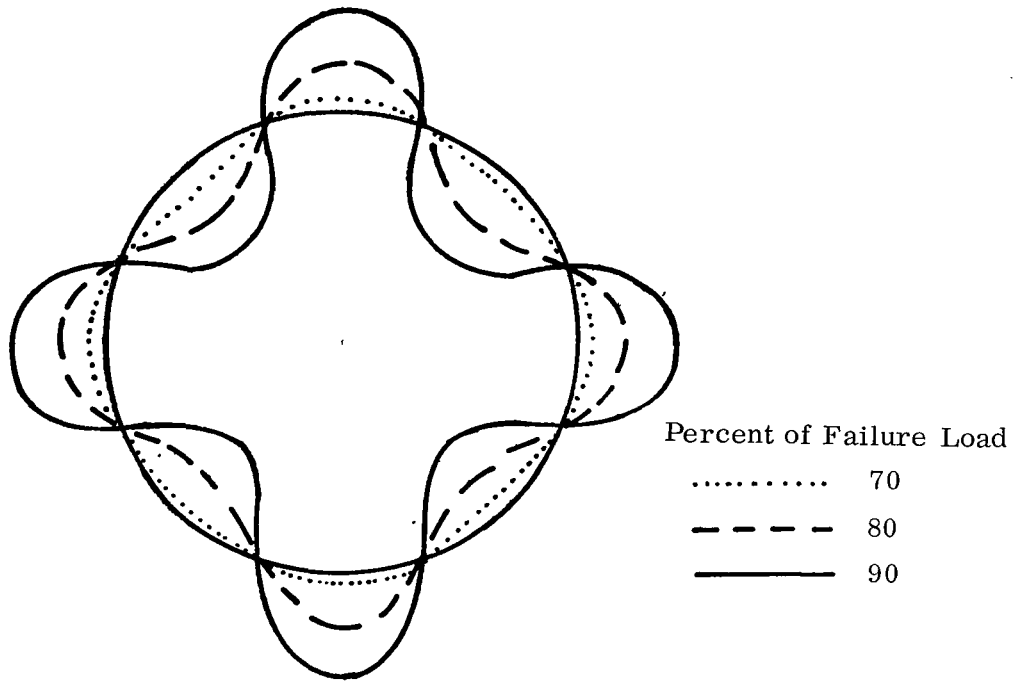


FIGURE 6. CIRCUMFERENTIAL MODE SHAPE OF CYLINDER TESTED IN AXIAL COMPRESSION

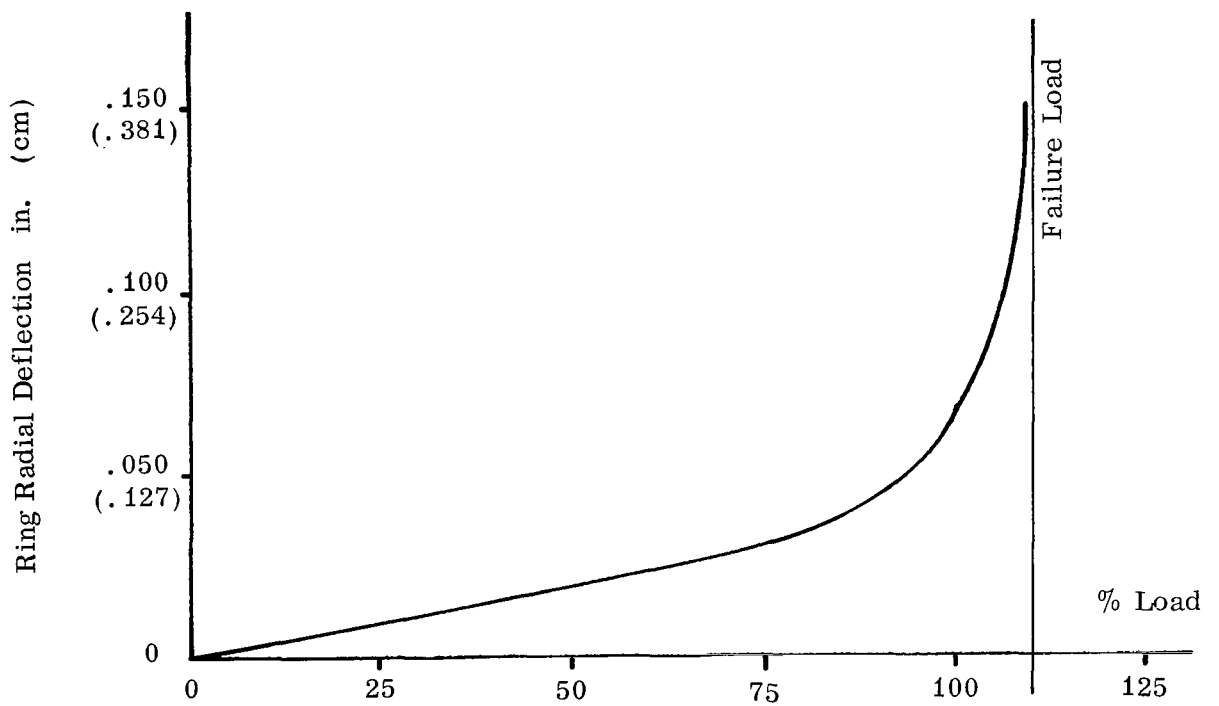


FIGURE 7. RING RADIAL DEFLECTION VERSUS PERCENT LOAD

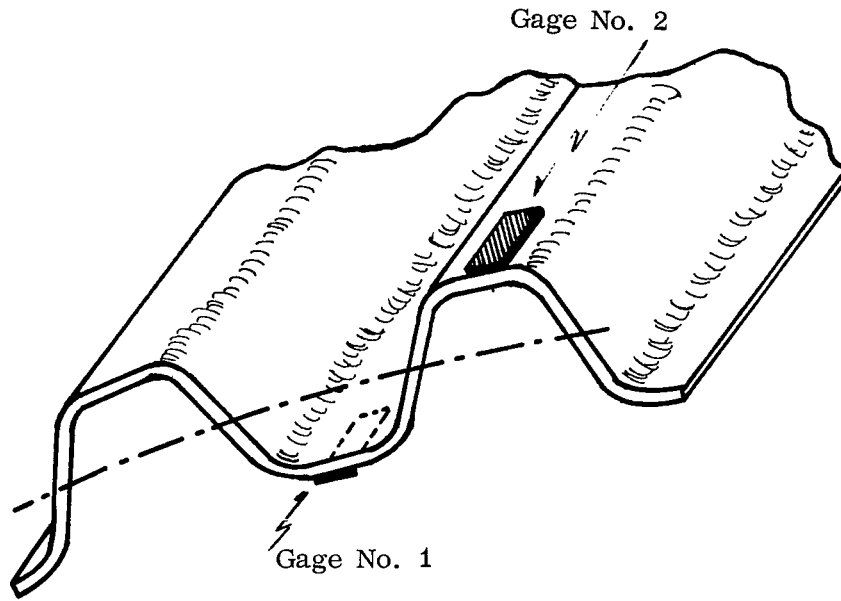


FIGURE 8. TYPICAL STRAIN GAGE LOCATIONS

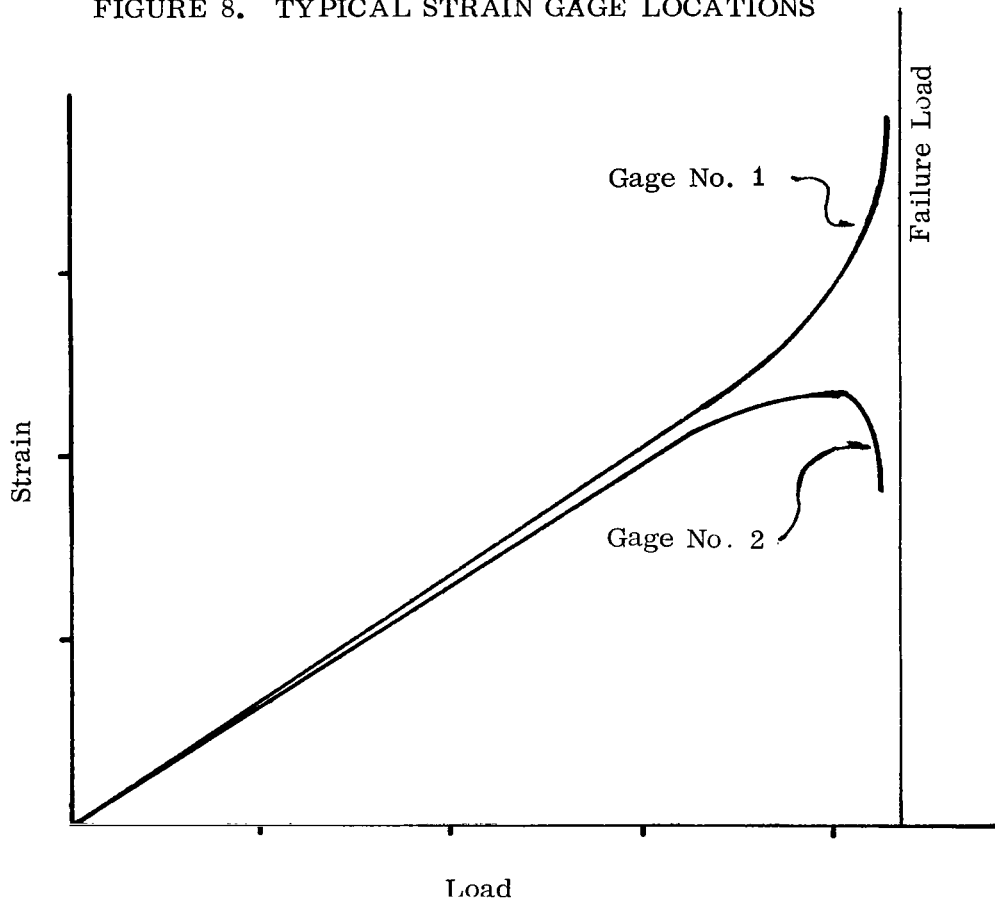


FIGURE 9. STRAIN VERSUS LOAD FOR TEST CYLINDER

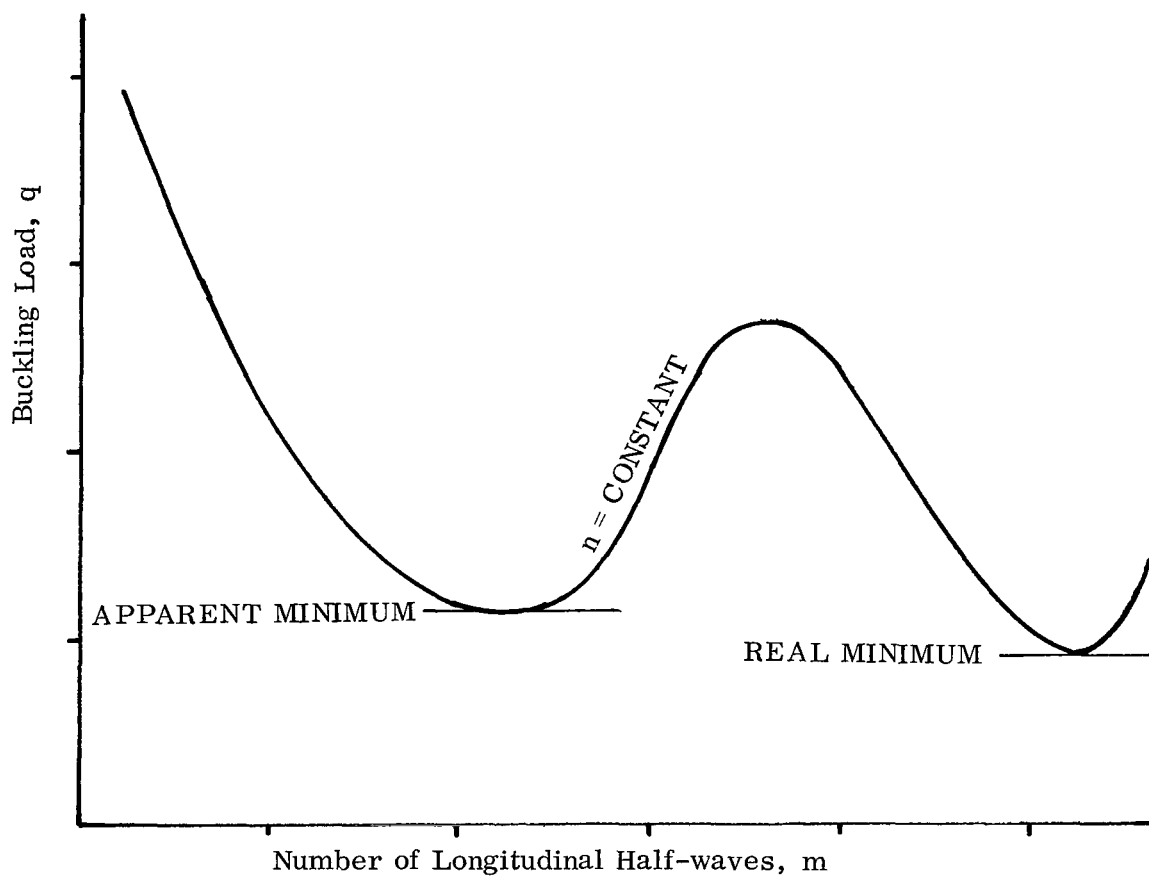


FIGURE 10. BUCKLING LOAD VERSUS MODE SHAPE, REAL AND APPARENT MINIMUMS

APPEND IX

The computer program is written in Fortran II. The program notation is given on page 24 and the program listing on pages 25 through 27. The sequence of steps for program compilation and operation is given in reference 10.

The program input data and corresponding column locations on the input cards are in the following form.

	1 - 19	20 - 69	70 - 80
Card 1	-	Case Title	-

	1-16	17-32	33-48	49-64	65-80
Card 2	E	ER	G	GR	R
Card 3	QL	TX	TS	QIX	C
Card 4	QLR	AR	QIYR	QIZR	QJR

	1-4	5-8	9-12	13-16	17-80
Card 5	M1	MM	N1	NN	-

where M1, N1 and MM, NN are the first and last values of m and n respectively, and

$$TX = t \text{ (D. F.)}$$

$$TS = t/\text{D. F.}$$

where D. F. , the development factor, is defined as the ratio of the average skin area per inch of circumference to the skin thickness.

An example of the program output is shown on pages 28 and 29. The axisymmetric mode shapes ($n = 0$) have been included for completeness.

In using the computer program a sufficient range of mode shapes must be considered so that the minimum buckling load is definitely obtained. This is mentioned because it is possible to have more than one apparent minimum buckling load as is shown in Figure 10.

COMPUTER PROGRAM NOTATION

TEXT NOTATION	PROGRAM NOTATION
a_{ij}	AIJ
c	C
m, n	QM, QN
\overline{m}	QMBAR
\overline{n}	QNBAR
q	Q3
t_x, t_s	TX, TS
A_r	AR
D_x, D_{yr}, D_{zr}	DX, DYR, DZR
E, E_r	E, ER
\overline{E}	EBARX
\overline{E}_R	EBARR
G, G_r	G, GR
\overline{G}	GBAR
I_x, I_{yr}, I_{zr}	QIX, QIYR, QIZR
J_r	QJR
K_r	QKR
L, L_r	QL, QLR
R, R_r	R, RR

THE GENERAL INSTABILITY OF RING STIFFENED CORRUGATED
CYLINDERS UNDER AXIAL COMPRESSION

```

1 READ 4
  READ 2, E, ER, G, GR, R, QL, TX, TS, QIX,
1    C, QLR, AR, QIYR, QIZR, QJR, M1, MM, N1, NN
  PUNCH 3
  PUNCH 4
  PUNCH 5
  PUNCH 12
  PUNCH 6
  PUNCH 7, E, ER, G, GR, R
  PUNCH 8
  PUNCH 9, QL, TX, TS, QIX, C
  PUNCH 10
  PUNCH 9, QLR, AR, QIYR, QIZR, QJR
  PUNCH 13
  PUNCH 14, M1, MM, N1, NN
  PUNCH 15
  PUNCH 16
  PUNCH 17
  PUNCH 18
  EBARX = F*TX
  GHAR = G*TS
  DX = E*QIX
  EBARR = ER*AR/QLR
  DYR = ER*QIYR/QLR
  DZR = ER*QIZR/QLR
  QKR = GR*QJR/QLR
  RR = R + C
  RRR = R/RR
  Y = 0
20 DO 51 N = N1, NN
  DO 51 M = M1, MM
  QM = M
  QN = N
  QMBAR = QM*3.14159/QL
  QNBAR = QN/R
  QR = R*C*QNBAR**2 + 1.
  QRR = -R*C*QNBAR**2 + 1./RRR
  A11 = -EBARX*QMBAR**2 - GBAR*QNBAR**2 - (DZR*QNBAR**2 + QKR/R**2)*
1    RRR**3*QNBAR**2
  A12 = GBAR*QMBAR*QNBAR
  A13 = - (DZR*QKR + QKR)*(RRR*QNBAR)**2*QMBAR/RR
  A22 = - GBAR*QMBAR**2 - (EBARR/RRR + DYR*RRR/R**2)*QNBAR**2
  A23 = - (EBARR*QNBAR*QK/R + DYR*QNBAR**3/RR)
  A33 = - DX*QMBAR**4 - (EBARR*GR**2/R**2 + DYR*QNBAR**4 + RRR**2*
1    (DZR*QKR**2/R**2 + QKR*QNBAR**2)*QMBAR**2)*RRR
  DD = QMBAR**6
  CC = QMBAR**4*(A11 + A22 + A33)
  BB = QMBAR**2*(A11*A22 + A11*A33 + A22*A33 - A12**2 -
1    A13**2 - A23**2)
  AA = A11*A22*A33 + 2.*A12*A13*A23 - A23**2*A11 - A13**2*A22

```

```

1      - A12**2*A33
      XXX = 0.
      Q1 = 0.
      E1 = DD*Q1**3 + CC*Q1**2 + BB*Q1 + AA
      DQ = .1*AA/((A12**2 - A11*A22)*(QMBAR**2))
21 Q2 = Q1 + DQ
22 E2 = DD*Q2**3 + CC*Q2**2 + BB*Q2 + AA
      IF (E1*E2) 28,28,26
26 Q1 = Q2
      E1 = E2
      GO TO 21
28 IF (XXX) 29,29,30
29 DQ = .01*Q2
      XXX = 1.
      GO TO 21
30 Q3 = Q1
      RAD = - 3.*(DD*Q3)**2 - 2.*DD*CC*Q3 + CC**2 - 4.*DD*BB
      IF (RAD) 50, 31, 31
31 Q4 = (-(CC + DD*Q3) + SQRTF(RAD))/(2.*DD)
      Q5 = (-(CC + DD*Q3) - SQRTF(RAD))/(2.*DD)
      IF (Q4) 34, 34, 32
32 IF (Q3 - Q4) 34, 34, 33
33 Q3 = Q4
34 IF (Q5) 50, 50, 35
35 IF (Q3 - Q5) 50, 50, 36
36 Q3 = Q5
50 P = 6.28*R*Q3
      STRES = Q3/TX
      IF (Y) 55, 55, 52
55 STREX = STRES
      MX = M
      NX = N
      GO TO 54
52 IF (STRES - STREX) 53, 51, 51
53 STREX = STRES
      MX = M
      NX = N
      GO TO 51
54 Y = 1.
51 PUNCH 19, Q3, P, STRES, M, N
      PUNCH 23
      PUNCH 24
      PUNCH 11, STREX, MX, NX
      GO TO 1
2 FORMAT (4F16.0, F16.4/ 5F16.4/ 5F16.4/ 4I4)
3 FORMAT (///19X41H THE GENERAL INSTABILITY OF RING STIFFENED/
119X44H CORRUGATED CYLINDERS UNDER AXIAL COMPRESSION//)
4 FORMAT (19X49H
5 FORMAT (///35X10H INPUT DATA)
6 FORMAT (15X1HE, 14X2HER, 15X1HG, 14X2HGR, 15X1HR)
7 FORMAT (4F16.0, F16.4//)
8 FORMAT (14X2HQL, 14X2HTX, 14X2HTS, 13X3HQIX, 15X1HC)

```

```

9 FORMAT (5F16.6//)
10 FORMAT (13X3HQLR, 14X2HAR, 12X4HQIYR, 12X4HQIZR, 13X3HQJR)
11 FORMAT (4XF16.4, 2(7XI3))
12 FORMAT (35X10H////////////////)
13 FORMAT (14X2HM1, 14X2HMM, 14X2HN1, 14X2HNN)
14 FORMAT (4(12XI4)///)
15 FORMAT (35X11HOUTPUT DATA)
16 FORMAT (35X11H////////////////)
17 FORMAT (15X5HAXIAL)
18 FORMAT (7X13HLOAD PER INCH, 10X10HAXIAL LOAD, 8X12HAXIAL STRESS,
1      9X1HM, 9X1HN/)
19 FORMAT (3(4XF16.4), 2(7XI3))
23 FORMAT (///3X17HMIN. AXIAL STRESS)
24 FORMAT (2X18HIN THE ABOVE RANGE, 9X1HM, 9X1HN)
01 FORMAT (F16.4)
      END

```

THE GENERAL INSTABILITY OF RING STIFFENED
CORRUGATED CYLINDERS UNDER AXIAL COMPRESSION

CYLINDER NO. 1

INPUT DATA
//////////

E 10500000.	ER 10500000.	G 3900000.	GR 3900000.	R 24.6800
QL 32.950000	TX .026600	TS .015100	QIX .000775	C -.730000
QLR 6.375000	AR .040000	QIYR .005000	QIZR 0.000000	QJR 0.000000
M1 1	MM 4	N1 0	NN 5	

OUTPUT DATA
 //////////////////////////////////

AXIAL LOAD PER INCH	AXIAL LOAD	AXIAL STRESS	M	N
12335.0930	1911820.9000	463725.3000	1	0
3361.1760	520950.0100	126360.0000	2	0
2028.1123	514357.9300	76244.8230	3	0
1949.9041	302216.4100	73304.6650	4	0
9282.7585	1438738.4000	348975.8800	1	1
3016.5183	467531.3700	113402.9400	2	1
1902.2971	294857.7800	71514.9280	3	1
1877.6704	291020.8800	70589.1120	4	1
4857.0714	752799.4300	182596.6600	1	2
2262.2310	350624.0800	85046.2780	2	2
1626.4831	252089.2600	61145.9810	3	2
1736.1352	269084.2800	65268.2400	4	2
2125.2484	329393.0900	79896.5560	1	3
1445.5047	224039.3500	54342.2810	2	3
1284.3015	199054.4000	48282.0110	3	3
1551.2859	240434.4200	58319.0180	4	3
1219.6112	189028.0200	45850.0450	1	4
889.5332	137869.1100	33441.1000	2	4
1001.3810	155204.4400	37645.9020	3	4
1386.0445	214823.5900	52106.9360	4	4
1677.6855	260025.1400	63070.8830	1	5
758.9283	117626.6000	28531.1400	2	5
887.8293	137605.0100	33377.0410	3	5
1307.4159	202636.9100	49150.9730	4	5

MIN. AXIAL STRESS
 IN THE ABOVE RANGE
 28531.1400

M N
 2 5

REFERENCES

1. Shanley, F. R., Simplified Analysis of General Instability of Stiffened Shells in Pure Bending, Jour. Aer. Sci. vol. 16, no. 10, pp. 590-592, October 1949.
2. Van der Neut, A., The General Instability of Stiffened Cylindrical Shells under Axial Compression, Rep. S314, National Aeronautical Research Institute, Amsterdam, in Reports and Transactions Vol. XIII, 1947, pp. S57-S84.
3. Hedgepeth, J. M. and Hall, D. B., The Stability of Stiffened Cylinders, ER 13731, Space Systems Division, Martin Company, Baltimore, Md., December 1964.
4. Card, M. F., Preliminary Results of Compression Tests on Cylinders with Eccentric Longitudinal Stiffeners, NASA TM-X-1004, Sept. 1964.
5. Baruch, M. and Singer, J., Effect of Eccentricity of Stiffeners on the General Instability of Cylindrical Shells under Hydrostatic Pressure, Jour. Mech. Eng. Sci., Vol. 5, no. 1, pp. 23-27, March 1963.
6. Van der Neut, A., General Instability of Orthogonally Stiffened Cylindrical Shells, Collected Papers on Instability of Shell Structures - 1962, NASA TN-D-1510, pp. 309-321, 1962.
7. Flugge, W., Stresses in Shells, Springer-Verlag, Berlin/Göttingen/Heidelberg, 1960.
8. Almroth, B. O., Buckling of Orthotropic Cylinders Under Axial Compression, LMSC-6-90-63-65, Lockheed Missile and Space Company, Sunnyvale, California, June, 1963.
9. Seely, F. B. and Smith, J. O., Advanced Mechanics of Materials, Second Edition, Chapter 6, paragraph 51, John Wiley & Sons, Inc., New York, London, 1952.
10. IBM 1620 Fortran (with format), File Number 1620-25, Form C26-5619-4, IBM Product Publications Department, San Jose, California, 1963.